Prion protein expression and functional importance in developmental angiogenesis: role in oxidative stress and copper homeostasis.

Nadia Alfaidy, Sylvain Chauvet, Sandrine Andrei, Aude Salomon, Yasmina Saoudi, Pierre Richaud, Catherine Aude-Garcia, Pascale Hoffmann, Annie Andrieux, Jean-Marc Moulis, et al.

Original Research Communication

Prion Protein Expression and Functional Importance in Developmental Angiogenesis: Role in Oxidative Stress and Copper Homeostasis

Nadia Alfaidy[2,3,4], Sylvain Chauvet[1,2,3] , Sandrine Andrei[1,2,3], Aude Salomon[2,3,4], Yasmina Saoudi[3,7], Pierre Richaud[6], Catherine-Aude Garcia[1,2,3], Pascale Hoffmann[2,3,4,5], Annie Andrieux[3,7], Jean-Marc Moulis[1,2,3], Jean-Jacques Feige[2,3,4], and Mohamed Benharouga[1,2,3].

1 Centre National de la Recherche Scientifique (CNRS), LCBM-UMR 5249, Grenoble, France.
2 Commissariat à l'Energie Atomique (CEA), DSV-iRTSV, Grenoble, France.
3 Université Joseph Fourrier (UJF), Grenoble 1, France.
4 Institut National de la Santé et de la Recherche Médicale (INSERM), U1036, Grenoble, France.
5 Centre Hospitalier Régional Universitaire de Grenoble, Département de Gynécologie, Obstétrique et Médecine de la Reproduction, Grenoble, France.
6 Commissariat à l'Energie Atomique (CEA), DSV-IBEB/SBVME/LB3M, Cadarache, France.
7 Institut National de la Santé et de la Recherche Médicale (INSERM), Institut des Neurosciences (GIN)/U836, Grenoble, France.

Running Title: Role of PrP^C protein in developmental angiogenesis.

Address correspondence to:
Dr. Mohamed Benharouga
LCBM-UMR5249
DSV-iRTSV, CEA-Grenoble
17 rue des Martyrs, F-38054, Grenoble cedex 09, France
Téléphone: (33)-4-38-78-44-51
Fax: (33)-4-38-78-54-87
E-mail: mohamed.benharouga@cea.fr

Word count: 5418

Reference numbers: 42

Greyscale illustrations: 7

Color illustrations: 2 (online 2)

Abstract

Aim: It has been convincingly shown that oxidative stress and toxicity by deregulated metals, such as copper (Cu), are tightly linked to the development of preeclampsia and intrauterine growth retardation (IUGR), the most threatening pathologies of human pregnancy. However, mechanisms implemented to control these effects are far from being understood. Among proteins that bind Cu and insure cellular protection against oxidative stress is the cellular prion protein (PrP^C), a GPI-anchored glycoprotein, which we reported to be highly expressed in human placenta. Herein, we investigated the pathophysiological role of PrP^C in Cu and oxidative stress homeostasis *in vitro* using human placenta and trophoblast cells, and *in vivo* using three strains of mice [C57Bl6; PrP^C knockout mice (PrP-/-) and PrP^C overexpressing mice (Tga20)].

Results: At the cellular level, PrP^C protection against oxidative stress was established in multiple angiogenic processes; proliferation, migration and tube-like organization. For the animal models, lack (PrP-/-) or over-expression (Tga20) of PrP^C in gravid mice caused severe IUGR that was correlated with a decrease in litter size, changes in Cu homeostasis, increase in oxidative stress response, development of hypoxic environment, failure in placental function, and maintenance of growth defects of the offspring even five months after delivery.

***Innovation*:** PrP^C could serve as a marker for the idiopathic IUGR disease.

Conclusion: These findings demonstrate the stress-protective role of PrP^C during development, and propose PrP^C dysregulation as a novel causative element of IUGR.

Introduction

Cellular prion protein (PrP^C) is a surface GPI-anchored glycoprotein expressed in neural and non-neural tissues (28,36). Although PrP^C is ubiquitously expressed, and when conformationally altered is the causative agent of spongiform encephalopathy, its normal function is poorly understood (35). However, it is noteworthy that the PrP-deficient (*PrP-/-*) mouse is viable and does not display an overt phenotype (9,32).

It is well established that PrP^C binds copper (Cu) *in vitro* and *in vivo* (7). In addition, PrP^C has been reported to protect cells against oxidative stress and to prevent apoptosis (31). Recently, PrP^C has been also assumed to play a role in angiogenesis (42). However, direct evidences to support this hypothesis are still missing.

In the placenta, an organ in which angiogenic processes are of utmost importance, vascularization plays a key role for successful pregnancy as it ensures the establishment of the feto-maternal circulation. This process occurs due to the transformation of the utero-placental vasculature by extravillous trophoblasts (EVT), following their proliferation, migration, and invasion into the maternal decidua and spiral arteries (25). Abnormal trophoblast invasion of the spiral arteries is thought to give rise to relatively hypoxic placenta. This, in turn, promotes an exaggerated state of oxidative stress in this tissue. This hypoxia/oxidative stress alter placental villous angiogenesis leading to a poorly developed fetoplacental vasculature. Oxidative stress per se may also affect vascular reactivity, blood flow, and oxygen and nutrient delivery to the fetus, which ultimately may be compromised (23,33).

During hypoxia, a series of adaptive modifications of gene expression occur, particularly via HIF-1α which facilitates placental vascularization as well as trophoblast differentiation (10). Interestingly, PrP^C expression was reported to be induced by HIF-1α (26). The later has also been shown to be activated by Cu (17).

Angiogenic processes are under the tight regulation of growth factors and metal ions such as Cu (13,14). Cu has been reported to stimulate the proliferation and migration of endothelial cells both *in vitro* and *in vivo* (29). Nevertheless, unlike classical angiogenesis, human placental angiogenesis requires only low levels of Cu for the establishment of the feto-maternal interface during the first trimester of pregnancy. Abnormally high levels of Cu have been associated with intrauterine growth restriction (IUGR) and preeclampsia (PE) (37), suggesting that Cu homeostasis must be critical for normal fetal and placental development.

Recently, we reported a high level of expression of PrP^C in human placenta that was restricted to the first trimester of pregnancy (16), suggesting a potential role of PrP^C in placental angiogenesis.

Based on the capacity of PrP^C to (i) bind Cu, (ii) respond to HIF-1α stimulus, and (iii) regulate endothelial cell migration and differentiation, we hypothesized that PrP^C is an important actor of the mechanisms that support the establishment of the feto-maternal circulation through a fine regulation of Cu homeostasis and oxidative stress, two hallmarks of IUGR. Both *in vitro* (human placenta and trophoblast cells) and *in vivo* studies on genetically modified PrP mice were conducted to investigate the role of PrP^C during development.

Results

Characterisation of PrP^C expression and maturation in throphoblast cells

We first examined the expression of PrP^C during the first trimester of pregnancy in human placental villi and placental columns, where EVT are detected. Compared to negative controls (Fig.1A-c and -d), PrP^C was expressed in primary EVT (Fig.1A-b), with a strong expression in placental columns at the anchoring site, particularly in the proliferative trophoblasts (Fig.1A-a and- b). Similar results were also observed in isolated EVT (Fig. S2).

To further characterize PrP^C expression, we used a well established anchoring trophoblast cell line; the HTR cells (18). Using RT-PCR, we showed that PrP^C gene is highly expressed in HTR compared to transfected BHK-21 cells stably expressing human PrP^C (Fig.1B). Immunoblot analysis showed the expression of PrP^C isoforms that correspond to the unglycosylated (U~21 kDa), the immature glycosylated (I~27 kDa), and the mature highly glycosylated PrP (H~33 kDa) (Fig.1C). As previously reported (34,10), PrP^C glycosylation was sensitive to N-glycosidase F (F) and insensitive to endoglycosidase H (H) (Fig.1D), and its cell surface expression profile was confirmed using non- and permeabilized HTR (Fig. 1E), sustaining the expression of mature PrP^C protein in HTR cells.

Cu and hypoxia upregulate PrP^C expression in trophoblast cells

We first analyzed the time and dose-dependent effect of Cu on PrP^C expression. PrP^C protein levels (Fig. 2A) were quantified and normalized based on the levels of the alpha (α) subunit of Na^+/K^+-ATPase (Fig.S3A). As shown in Fig. 2A, PrP^C was detected in untreated HTR as U-, I- and H-glycosylated forms. Following Cu stimulation, only the I- and H-glycosylated forms gradually increased after 14h and 24h of treatment, respectively (Fig. 2A and Fig. S3A). Similar results have also been observed using 50 and 200, but not 10 μM of Cu (Fig.S3B). Like PrP^C protein expression, the PrP^C mRNA levels significantly increased in response to Cu (Fig.2B). The high level of H-glycosylated forms of PrP^C observed following Cu treatment suggested an increase of PrP^C insertion into plasma membrane. This hypothesis was confirmed by cell surface biotinylation assays showing that Cu treatment increased the plasma membrane insertion of PrP^C (Fig. 2C). Image analysis revealed that the abundance of biotinylated PrP^C was increased gradually to reach ~ 90% at 24h (Fig. 2D).

Finally, we found that hypoxia significantly increased the expression of PrP^C at the mRNA and protein levels both in primary trophoblast and HTR cells (Fig.S4A and B).

PrP^C protects against Cu accumulation, Cu-induced ROS production, and trophoblast death.

The increase of PrP^C expression upon Cu treatment may reveal the presence of a stress protective response. To evaluate this hypothesis, we monitored ROS accumulation, catalase activity, intracellular Cu content, and cell death following Cu treatment in the absence or presence of PrP^C. The cellular prion protein was knocked down using siRNA to PrP^C. The efficiency of the PrP^C knockdown was demonstrated both at the mRNA and protein levels (Fig. S5A and B). After exposure of HTR cells to 50 and 100 µM of Cu, the DCF fluorescence, indicative of ROS production, increased compared to untreated HTR (Fig. 3A). In the PrP-silenced HTR, the level of DCF fluorescence was similar compared to the control HTR (Fig. 3A). The treatment of PrP-knockdown HTR with 50 and 100 µM of Cu increased ROS accumulation by 5.5- and 7.7-fold, respectively (Fig. 3A).

To determine whether the increased levels of ROS induced by Cu in PrP-silenced HTR (Fig. 3A) can modulate the antioxidant status of these cells, we evaluated the activity of catalase (CAT), an antioxidant reductase of H_2O_2. The absence of PrP^C did not affect the CAT activity that was increased by ~2- and ~5-fold, following Cu treatment, in normal and PrP-silenced HTR, respectively (Fig. 3B). By binding Cu, PrP^C might regulate the intracellular Cu concentration. To test this hypothesis, we employed ICP-AES to measure Cu concentration in normal and PrP-knockdown HTR before and after cellular exposure to Cu. The results indicated a concentration of ~0.2 µmoles/10^6 cells for normal HTR (Fig. 3C). A slightly elevated copper level (~0.3 µmoles/10^6 cell) was detected in PrP-silenced HTR cells (Fig. 3C). When Cu was added during 24h, the intracellular copper concentration was increased to ~10 and ~20 µmoles/10^6 cell in wild type and PrP-depleted HTR, respectively (Fig. 3C).

To test the role of elevated PrP^C expression in preventing the cytotoxicity induced by Cu, we measured the effects of Cu on cellular viability using trypan blue staining. After 32h incubation with Cu, wild type HTR exhibited a basal cell death of ~20% (Fig. 3D, *filled triangles*). Depletion of PrP^C had no significant effect on cell survival (~15.6% at 32h) (Fig. 3D, *open circle*). A significant increase in cell death was, however, observed in PrP-depleted HTR (~30% at 32h) following incubation with Cu (Fig. 3C, *open triangles*).

PrP^C attenuates the effect of Cu on trophoblasts angiogenic processes

We examined whether silencing PrP^C expression, in the presence or absence of Cu, would affect the three angiogenic processes undertaken by trophoblasts during their establishment of fetomaternal circulation, ie: proliferation, migration and tube-like organization.

In HTR, the three processes were unaffected by 5 and 10 µM of Cu (Fig. S6A and B), while, as reported previously (13), this treatment stimulates proliferation and migration of human umbilical vein endothelial cells (HUVEC) (Fig. S6C and D).

EVT invasion is accompanied by endovascular differentiation wherein EVT finally replaces endothelial cells in uterine vessels. Using time lapse microscopy, we investigated the role of PrP^C on tube-like formation by HTR cells (Fig. 4A and B). In the control condition, HTR start to organize into tube-like structures by 6h. By 24h of culture all cells were organized in a network of tubular structures. 100 µM of Cu significantly delayed this organization as it did not start until after 18h of incubation. Silencing PrP^C expression did not affect this organization. In contrast, in PrP^C-silenced HTR, Cu completely inhibited the cell organization. As a positive control, we showed that FGF-2, a potent angiogenic factor, induced a rapid organization of HTR (Fig 4A and B). To quantify the effect of Cu on HTR organization, we determined the number of capillary networks formed under different conditions. As shown in Figure 4B, Cu significantly decreased the number of tube-like structures. This effect was amplified in the absence of PrP^C. A movie of tube-like structure formation is provided (see movie S1). Similarly, the inhibitory effect of Cu on the closure of wounded HTR and on the number of HTR cells was exacerbated in the absence of PrP^C (Fig. 5A, B and C).

In order to test the specificity of the copper effect, HTR cells were treated with hemin as a source of iron in similar experiments as reported above. The obtained results with hemin were generally opposite to those with copper (not shown) and their significance is presently under study.

PrP^C overexpression affects HTR angiogenic processes

As reported in figure 3, the knock down of PrP^C protein exacerbated the inhibitory effect of Cu on multiple HTR angiogenic processes and created an oxidative stress environment that was harmful for HTR cells (Fig. 3). However, it is well established that Cu over-chelation affects Cu/Zn SOD activity that consequently increase ROS production and cell death (5,20), suggesting that overexpression of a Cu-high affinity binding protein, such as PrP^C, might also impact the cellular antioxidant balance.

To test this hypothesis, we overexpressed PrP^C protein in HTR cells and evaluated its impact on ROS production, cells mortality, and HTR angiogenic processes such as migration and proliferation. PrP^C overexpression was achieved by transient transfection of GFP-hPrP^C fusion protein, followed, 24h later, by fluorescent cell sorting to enrich GFP expressing HTR cell population. The overexpression was confirmed by the increase (~6 fold) of PrP^C

expression in HTR cells detected by immunoblot using an anti-PrP (Fig. 6A) and an anti-GFP (Fig. 6B) antibody. Both antibodies recognized the H, I and U forms of the PrP^C protein at the corresponding molecular weights (Fig. 6A and B).

The transfected cells were then assessed for their proliferation, migration, cell mortality profile, and for their ROS production. First, we observed a significant decrease in HTR cells proliferation and a significant increase in their mortality compared to the control cells that were transiently transfected with a mock plasmid (Fig. 6C). Those effects were the consequence of the establishment of an oxidative stress environment as confirmed by ROS measurement (Fig. 6D). The production of ROS was significantly attenuated in the presence of 5 µM of Cu (Fig. 6D), a concentration that does not affect PrP^C protein expression.

Our results showed that addition of Cu partially reverse the effect of PrP^C overexpression, suggesting that Cu could be chelated by PrP^C at the cell surface which leads to a reduction in free copper, leading to ROS production that is harmful to HTR cells. Next, we tested the effect of PrP^C overexpression on the main angiogenic process, the wound healing assay, in the absence or presence of 5 µM copper. As illustrated in figure 6E and 6F, PrP^C transfected cells exhibited a significant delay in their wound closure compared to the control transfected cells. Interestingly, in the presence of Cu the inhibitory effect on the wound closure was lessened and addition of Cu significantly improved the migration of the cells (Fig. 6E and F). These results further support a direct relationship between PrP^C expression levels and Cu.

To substantiate our cellular results and get more insight into the physiological role of PrP^C in the outcome of pregnancy, we undertook *in vivo* studies. We took advantage of the availability of two strains of mice with a C57Bl6 background that were generated to study the role of PrP^C in the transmission of prion disease; the PrP^C knockout mice (PrP-/-) and the PrP^C overexpressing (Tga20) mice.

Tga20 and Prnp-/- mice showed pronounced defects in their litter size, growth, and offspring growth

First we showed, as previously reported for humans placentas (16), that PrP^C was highly expressed at the mRNA and protein levels in the placentas of wt mice during early gestation, corresponding to the age of the establishment of foetomaternal circulation (Fig. S7A and B).

Then, we evaluated the efficiency of Cu treatment by measuring blood Cu concentration at different gestational ages in the three strains of mice. As reported for humans (4), circulating Cu concentrations increased gradually throughout gestation from ~0.45 µg/ml up to ~0.95 µg/ml (Fig. 7A). Compared to wt and Tga20, PrP-/- mice had a two-fold higher blood Cu

concentration (Fig. 7A). The later increased only in the blood of gravid wt and PrP-/- mice following Cu treatment (Fig. 7A).

Regarding the litter size, no significant change was observed in PrP-/- compared to wt mice in the absence of Cu treatment (Fig. 7B). However, a significant decrease was observed in the Tga20 (Fig. 7B). Increasing circulating Cu concentrations did not affect the litter size of Tga20 or PrP-/- mice, but did significantly decrease the number of embryos in the wt group (Fig. 7B).

We then compared the fetal and placental weights, and the placental efficiency in all groups at E14.5 and E17.5. In the absence of Cu, only the PrP-/- showed a significant decrease in fetal and placental weights at E17.5 (Fig. 7C-a, -b, -c and -d). Following Cu treatment, none of the two parameters was affected in wt and Tga20 mice, but both decreased in the PrP-/-, except for placental weight which showed a significant increase at E17.5 (Fig. 7C-a, -b, -c and -d).

In the PrP-/- group, the changes in fetal and placental weights in the absence or presence of Cu was confirmed by the decrease in placental efficiency (Fig. 7C-e and 7C-f).

As shown above, a lack or an over-expression of PrP^C caused severe IUGR and a significant decrease in the litter size, respectively. Hence, we wondered whether the developmental changes observed in PrP-/- and Tga20 mice had any impact on their offspring at the adulthood. Figure 7D shows a follow up of the body weight of offspring from wt, Tga20 and PrP-/- during five months. Tga20 and PrP-/- offspring's exhibited significant lower body weights in their adulthood compared to wt offspring.

Correlation between structural changes in placentas and placental gene expression

Histology was performed to compare the placental structure of the three groups of gravid mice. Tga20 labyrinth structure was comparable to that of the wt, but there was an apparent compaction of the labyrinth of PrP-/- placentas (Fig. S8A and B). As the labyrinth is the major site of nutrient and gas exchange, we compared the vascularization of this zone between the three groups using CD31, an endothelial cell marker. Both Tga20 and PrP-/- showed an apparent disorganization of the vascular tree within their labyrinth (Fig. 8A). These results were confirmed by immunoblot in the absence or presence of Cu (Fig. 8B and C). In the presence of Cu, CD31 levels increased in wt and Tga20, but did not change in the PrP-/- (Fig. 8B and C). Furthermore, placental growth defects observed in the Tga20 and PrP-/- mice were confirmed by changes in the surface area of the main zones of the placenta (labyrinth layer, spongiotrophoblast and decidua) determined at E14.5 (Fig. S9).

Based on the significant functional and structural changes observed in placentas from Tga20 and PrP-/- mice, we evaluated the expression profile of specific genes with roles in the formation of specific placental structures such as proliferin, a marker for invasive trophoblasts, Mash2, a marker for spongiotrophoblast, Gcm1, important for labyrinth branching, and CD31, (2,19). RT- PCR revealed that placental expression of Proliferin and Mash2 were significantly down regulated in the Tga20 mice, and were highly expressed in PrP-/- mice (Fig. 8D). Treatment with Cu reversed the decrease observed in Tga20 for both genes (Fig. 8D). There was a trend to a decrease in the expression of these genes in the PrP-/- treated group without reaching significance (Fig. 8D). Analysis of Gcm1, showed an increase in its expression in placentas from Tga20 and PrP-/- that was significant in the PrP-/- mice. Cu treatment significantly increased Gcm1 expression in the wt group (Fig. 8D). At 17.5 dpc, only the PrP-/- group conserved the significant increase in Gcm1 gene. Figure 8D shows also that CD31 mRNA was more abundant in the PrP-/- group, with a significant decrease in the Tga20 group at 10.5 dpc. There was a trend to a normalization of CD31 levels in both groups after Cu treatment; however this did not reach significance (Fig. 8D).

Evidence for sustained placental hypoxia in Tga20 and PrP-/- placentas

Maintenance of a hypoxic environment beyond 10.5 dpc is a sign of placental endurance. To assess the degree of hypoxia, we evaluated the levels of HIF-1α protein expression. As expected in wt mice, HIF-1α expression was highest at 10.5 and decreased by 14.5 dpc. Interestingly Cu supplementation increased HIF-1α expression both at 10.5 and 14.5 dpc, suggesting maintenance of the hypoxic environment (Fig. 9A and B). In PrP-/- and Tga20 mice, HIF-1α expression was significantly higher at 10.5 as compared to wt mice suggesting an existing hypoxic environment and therefore a basal placental endurance in the absence of any treatment. Cu supplementation exacerbated this phenomenon in Tga20 mice, with a slight increase in PrP-/- mice, both at 10.5 and 14.5 (Fig. 9A and B).

Discussion

Here, both *in vitro* and *in vivo* studies i) demonstrate the role of PrP^C in placental Cu homeostasis and protection against oxidative stress, ii) reveal a new role of PrP^C in normal and pathological pregnancies, and iii) bring forth evidence suggesting that PrP^C is directly involved in placental angiogenesis. These statements are based on several key findings. First, Cu treatment leads to a dose-dependent increase of PrP^C expression in trophoblast cells (Fig.2). Second, the knockdown of PrP^C, which is endogenously expressed in the trophoblasts, deprives the cells from protection against external stressors, such as Cu overload, a condition that completely inhibits their proliferation, migration, tube like organization, and increased their level of oxidative stress. (Fig.3). Third, the overexpression of PrP^C also increases ROS production and causes deleterious effects on the trophoblasts basic angiogenic processes, including proliferation and migration. Hence, we demonstrate, *in vitro*, that both the knockdown and the overexpression of PrP^C critically affected trophoblast angiogenic function by contributing into Cu and oxidative stress homeostasis.

In this study, we have shown that Cu increased PrP^C plasma membrane insertion, demonstrating a direct relationship between PrP^C and Cu and suggesting that PrP^C might play a role as a Cu sensor and/or chelator at the cell surface to protect trophoblasts from Cu excess.

The demonstration that PrP^C protects trophoblasts against Cu overload is of great physiological interest since Cu levels are known to increase during the first trimester of pregnancy and is abnormally increased in IUGR and PE. These results are in line with recently published data (22) showing a significant increase of PrP^C in PE. We have also demonstrated that PrP^C is abundant in primary trophoblasts and in HTR cells subjected to hypoxia, and we know that hypoxia is central to IUGR and PE pregnancies, suggesting that the increase in PrP^C expression in PE might also be a response to the hypoxic environment usually associated to these pathologies.

Our *in vivo* approach has provided strong evidence in support of this hypothesis, as we observed a direct involvement of PrP^C protein in placentation and pregnancy outcomes.

The most striking findings are the direct consequences of the loss or gain of the PrP^C protein expression on fetal growth and litter size. In the Tga20 strain, the significant decrease in their litter size might well be explained by an over chelation of Cu. In this tissue, the available Cu has probably been over-chelated by the surplus of PrP^C overexpression. Hence, Tga20 is a good model of the consequences of Cu chelation on the outcome of the pregnancy.

Our hypothesis was further supported by our *in vitro* data (Fig. 6) demonstrating that overexpression of PrP^C protein generates ROS production and impacts trophobalst angiogenic processes. Interestingly, the role of Cu chelation in ROS production and cell death has been reported by several groups (38,12,5,20). Also, overexpression of PrP^C, a high affinity Cu binding was associated with an increase in ROS production (24). In this study, the authors showed that in the thymus, circulating Cu and/or Cu from exocytosis could be chelated by PrP^C at the cell surface which leads to a reduction in free Cu, creating an oxidative stress environment that is harmful to the αβ T cell development in the Tga20 mice. They also showed that those effects were partially reversed by addition of Cu (24). Furthermore, HSV-1 (*Herpes simplex virus*) replication proceeds more efficiently in neuronal tissue that overexpresses PrP^C, suggesting that over chelation of Cu helps to generate an oxidative stress environment that serves to limit the pathogenesis of acute HSV-1 infection (40).

The significant decreases in the spongiotrophoblast and giant cell layers suggest a direct role of PrP^C in the development of the placental zones that control the invasion of trophoblast cells into the maternal decidua. These results are consistent with the strong and sustained increase in HIF-1α protein expression in Tga20 placenta at 10.5 and 14.5 dpc.

More importantly, we showed that Cu supplementation of Tga20 mice trended to normalize many aspects of these processes including the relief of the hypoxic environment at the later stages of gestation.

In contrast to the Tga20 mice, the PrP-/- strain showed a normal litter size, but developed IUGR. The occurrence of this pathology in the PrP-/- model further demonstrates the protecting role that PrP^C plays to insure successful pregnancy.

The gestation of the PrP-/- mice mimics a condition that might occur in IUGR pregnancies, as these pathologies are often associated with an increase in circulating Cu and oxidative stress. The PrP-/- model, not only revealed the precise role for PrP^C protein in placentation, but brought direct evidence for placental adaptations under abnormal circumstances. In fact, in the PrP-/- model the decrease in fetal weight observed at E14.5 was less apparent at day 17.5. This was the result of an increase in placental efficiency at E17.5 that was not sufficient to overcome the sustained decrease in fetal weight, confirming placental endurance in the absence of PrP^C. The changes in the expression of the genes that control branching of the labyrinth, such as Gcm1 and CD31, further demonstrate that the PrP-/- placenta has adapted its response to high circulating Cu to ensure a normal fetal development.

Although the structural and functional changes in the PrP-/- and Tga20 models enabled adaptation and survival of this strains, we demonstrated that these changes affected their

offspring with severe impact on their growth. Even if the Tga20 fetuses did not show a significant change in their weight during gestation, their offspring showed a significant, but less marked, decrease in their body weight compared to that observed in the offspring of PrP-/- mice. Further evidence for PrP^C protection of the developing placenta from Cu excess and oxidative stress comes from the data obtained after Cu supplementation. Altogether the *in vivo* results are in accordance with our *in vitro* data showing a high sensitivity of trophoblast cells to PrP^C levels.

In conclusion, we have demonstrated the physiological role of PrP^C in placental angiogenesis during pregnancy, and propose PrP^C normal expression as a major aspect for its success. By regulating Cu content and oxidative stress, PrP^C contributes to the control of these key parameters often associated to major pregnancy pathologies such as IUGR.

Innovation:

To date the physiological function of the cellular prion is still not clear.

Here, we report a role for PrP^C in the success of pregnancy. PrP^C dysregulation (loss or gain) cause irreversible effects on pregnancy outcome, and affect key angiogenic processes necessary for the establishment of the fetomaternal circulation and for the growth of the placenta. These findings bring new insights into the fine regulation of developmental processes by Cu, and into the origin of the oxidative stress often associated to placental pathologies such as IUGR.

Experimental Procedures

Tissue collection:

First trimester human placentas from 7 to 12 weeks of gestation (wg) were collected as previously described (16). Collection and processing of human placentas was approved by the University Hospital ethics committee and informed consent was obtained from each patient. For the *in vivo* experiments, mice (8–10 weeks old; 20-25 g) of three strains C57 wild type (wt), Prnp-KO (PrP-/-) (8,9), and Tga20/Tga20 (Tga20) (41) were used. The transgenic mice were obtained from the animal facility of CNRS (Orleans, France). As our study mainly used placental tissues, we have reported an *in situ* experiment that compares the local expression of PrP^C protein in the placenta of wt, PrP-/- and Tga20 mice both at 10,5 and 14,5 dpc (Fig. S1). All procedures involving animals and their care were approved by the local institutional Ethics Committee. Mice were sacrificed using cervical dislocation following chloral hydrate anesthesia. Fresh placenta, fetus and liver were collected from each animal. Shortly after collection, tissues were snap-frozen in dry ice and stored at -80°C (for RNA and protein extraction), or fixed in 4% paraformaldehyde (PFA) at room temperature (for immunohistochemistry).

Copper dietary supplementation and body weights of the offspring

The gravid mice (wt, Tga20, PrP-/-) were randomly assigned to receive either distilled water containing 50 ppm sucrose or 250 ppm copper (copper sulfate ($CuSO_4$)) and 50 ppm sucrose. The diet was maintained throughout the experimental period. Gravid mice were sacrificed at E10.5, E14.5 or E17.5 dpc (days post coïtum), and the blood was drawn by cardiac puncture just before laparotomy was performed. In another set of experiments three mice from each group (wt, Tga20, PrP-/-) were allowed to give birth and the body weights of their offspring were measured every week for up to 5 months.

Placental histology and embryo weight

The relative cross-sectional areas of E14.5 and E17.5 placentas were determined from H&E stained sections. Quantitative analysis of the placental areas of 20×magnification captured images was performed using the imageJ program (NIH, http://imagej.nih.gov). A single section from the center of each placenta was used, based on the site of umbilical attachment. Placentas and embryos were weighed at E14.5 and E17.5 dpc, and average weights were analyzed as raw weights.

Immunohistochemistry

Immunohistochemistry was performed as described previously (16). See Supplemental Experimental Procedures for details.

Isolation of primary cytotrophoblast and cell culture

Placental cytotrophoblasts (CT) isolated from first-trimester human placentas (10-12 wk of gestation, n =6) and trophoblast-derived HTR-8/SVneo cells, kindly provided by Dr. Charles H. Graham (Queen's University, Kingston, ON, Canada), were cultured as previously reported (21). See Supplemental Experimental Procedures for details.

siRNA knockdown of PrP^C and Transfection

The silencing PrP^C expression essay was performed following the protocol described in a previous report (6). See Supplemental Experimental Procedures.

Construction of EGFP–$hPrP^C$ expression vector

Generation of the EGFP-human PrP^C (GFP-$hPrP^C$) fusion protein was previously described (15).

Cell lines and transfection

HTR cells were transiently transfected with EGFP-$hPrP^C$ tagged protein and sorted, 24h after transfection, in fluorescence-activated cell sorting apparatus (FACS) to enrich the GFP expressing cell population as described previously (15). After sorting, the cells were seeded and 24h later used for the indicated experiments.

Cell proliferation, cell wound-healing and Tube-like formation assay

HTR migration, proliferation and tube-like formation capacity were evaluated on the normal and PrP^C siRNA knockdown HTR, as previously reported (6). See Supplemental Experimental Procedures for details.

Immunofluorescence microscopy

The indirect immunofluorescence has been done as described previously (15). See Supplemental Experimental Procedures for details.

Biochemical essays

Electrophoresis and immunoblotting, endoglycosidase digestion, and cell surface biotinylation has been conducted as described previously (15,16). See Supplemental Experimental Procedures for details.

RNA isolation, reverse Transcriptase and Real-Time Polymerase Chain Reaction analysis

Total RNA was extracted from HTR cells and mice tissues samples and reverse transcription was performed under conditions recommended by the manufacturer (Invitrogen, Cergy Pontoise, France). Prion, GCM1, Mash2, proliferin, CD31, GAPDH mRNAs, and 18S rRNA

expression were quantified by real-time RT-PCR. The PCR was performed using the primers shown in Table S1. See Supplemental Experimental Procedures for details.

Intracellular copper determination, ROS Measurements and Catalase enzyme activity assays

To evaluate the intracellular copper concentration, HTR cells, serum, and tissue samples (maternal liver and placenta) from C57, PrP-/- and Tga20 mice were collected and stored at -80 ℃. Copper concentration, ROS measurements and *catalase enzyme activity were determined according to previously reported protocol* (3,30,34). See Supplemental Experimental Procedures for details.

Statistical analysis

Statistical comparisons were made using one-way ANOVA analysis and tested for homogeneity of variance and normality ($p < 0.05$). Student's t-test was also used when appropriate. Calculations were performed using SigmaStat (Jandel Scientific Software, SanRafael, CA).

Acknowledgments

We thank the staff of the Department of Gynecology/Obstetrics (Pr. F. Sergent) at the University Hospital of Grenoble for giving us access to human placentas. We also thank Mr. Frederic SERGENT for his assistance with the animal work. We acknowledge the following sources of funding: CNRS (LCBM-UMR 5249); INSERM (U1036), UJF, and CEA/DSV/iRTSV).

Author Disclosure Statement

There is no conflict of interest.

List of Abreviations

Cu: Copper

DCF: dichlorofluorescein

EVT: ExtraVillous Trophoblasts

GPI: Glycosyl Phosphatidyl Inositol

HIF-1α: Hypoxia Inducible Factor 1-alpha

IUGR: Intrauterine Growth Retardation

PE: Preeclampsia

PrP^{C}: Cellular Prion Protein

ROS: Reactive Oxygen Species

EGFP: Enhance Green Fluorescent Protein

References

1. Al-Saleh E, Nandakumaran M, Al-Shammari M, Al-Falah F, Al-Harouny A. Assessment of maternal-fetal status of some essential trace elements in pregnant women in late gestation: relationship with birth weight and placental weight. *J Matern Fetal Neonatal Med* 16: 9-14, 2004.

2. Basyuk E, Cross JC, Corbin J, Nakayama H, Hunter P, Nait-Oumesmar B, Lazzarini RA. Murine Gcm1 gene is expressed in a subset of placental trophoblast cells. *Dev Dyn* 214: 303-11, 1999.

3. Beers, R.F., Jr., and Sizer, I.W. 1952. A spectrophotometric method for measuring the breakdown of hydrogen peroxide by catalase. *J Biol Chem* 195:133-140.

4. Borella P, Szilagyi A, Than G, Csaba I, Giardino A, Facchinetti F. Maternal plasma concentrations of magnesium, calcium, zinc and copper in normal and pathological pregnancies. *Sci Total Environ* 99: 67-76, 1990.

5. Borrello S, De Leo ME, Landriscina M, Palazzotti B, Galeotti T. Diethyldithiocarbamate treatment up regulates manganese superoxide dismutase gene expression in rat liver. *Biochem Biophys Res Commun* 220: 546-552, 1996.

6. Brouillet S, Hoffmann P, Benharouga M, Salomon A, Schaal JP, Feige JJ, Alfaidy N. Molecular characterization of EG-VEGF-mediated angiogenesis: differential effects on microvascular and macrovascular endothelial cells. *Mol Biol Cell* 21: 2832-43.

7. Brown DR, Qin K, Herms JW, Madlung A, Manson J, Strome R, Fraser PE, Kruck T, von Bohlen A, Schulz-Schaeffer W, Giese A, Westaway D, Kretzschmar H. The cellular prion protein binds copper in vivo. *Nature* 390: 684-7, 1997.

8. Bueler H, Aguzzi A, Sailer A, Greiner RA, Autenried P, Aguet M, Weissmann C. Mice devoid of PrP are resistant to scrapie. *Cell* 73: 1339-47, 1993.

9. Bueler H, Fischer M, Lang Y, Bluethmann H, Lipp HP, DeArmond SJ, Prusiner SB, Aguet M, Weissmann C. Normal development and behaviour of mice lacking the neuronal cell-surface PrP protein. *Nature* 356: 577-82, 1992.

10. Burton GJ. Oxygen, the Janus gas; its effects on human placental development and function. *J Anat* 215: 27-35, 2009.

11. Buschmann A, Kuczius T, Bodemer W, Groschup MH. Cellular prion proteins of mammalian species display an intrinsic partial proteinase K resistance. *Biochem Biophys Res Commun* 253: 693-702, 1998.

12. Byrnes RW, Mohan M, Antholine WE, Xu RX, Petering DH. Oxidative stress induced by a copper-thiosemicarbazone complex. *Biochemistry* 29: 7046-7053, 1990.

13. Camphausen K, Sproull M, Tantama S, Venditto V, Sankineni S, Scott T, Brechbiel MW. Evaluation of chelating agents as anti-angiogenic therapy through copper chelation. *Bioorg Med Chem* 12: 5133-40, 2004.

14. Carmeliet P, Jain RK. Molecular mechanisms and clinical applications of angiogenesis. *Nature* 473: 298-307.

15. De Keukeleire, B., Donadio, S., Micoud, J., Lechardeur, D., and Benharouga, M. 2007. Human cellular prion protein hPrPC is sorted to the apical membrane of epithelial cells. *Biochem Biophys Res Commun* 354:949-954.

16. Donadio S, Alfaidy N, De Keukeleire B, Micoud J, Feige JJ, Challis JR, Benharouga M. Expression and localization of cellular prion and COMMD1 proteins in human placenta throughout pregnancy. *Placenta* 28: 907-11, 2007.

17. Feng W, Ye F, Xue W, Zhou Z, Kang YJ. Copper regulation of hypoxia-inducible factor-1 activity. *Mol Pharmacol* 75: 174-82, 2009.

18. Graham CH, Hawley TS, Hawley RG, MacDougall JR, Kerbel RS, Khoo N, Lala PK. Establishment and characterization of first trimester human trophoblast cells with extended lifespan. *Exp Cell Res* 206: 204-11, 1993.

19. Guillemot F, Nagy A, Auerbach A, Rossant J, Joyner AL. Essential role of Mash-2 in extraembryonic development. *Nature* 371: 333-6, 1994.

20. Hancock CN, Stockwin LH, Han B, Divelbiss RD, Jun JH, Malhotra SV, Hollingshead MG, Newton DL. A copper chelate of thiosemicarbazone NSC 689534 induces oxidative/ER stress and inhibits tumor growth in vitro and in vivo. *Free Radic Biol Med* 50: 110-121, 2011.

21. Hoffmann P, Saoudi Y, Benharouga M, Graham CH, Schaal JP, Mazouni C, Feige JJ, Alfaidy N. Role of EG-VEGF in human placentation: Physiological and pathological implications. *J Cell Mol Med* 13: 2224-35, 2009.

22. Hwang, H.S., Park, S.H., Park, Y.W., Kwon, H.S., and Sohn, I.S. Expression of cellular prion protein in the placentas of women with normal and preeclamptic pregnancies. *Acta Obstet Gynecol Scand* 89:1155-1161.

23. Hunkapiller NM, Gasperowicz M, Kapidzic M, Plaks V, Maltepe E, Kitajewski J, Cross JC, Fisher SJ. A role for Notch signaling in trophoblast endovascular invasion and in the pathogenesis of pre-eclampsia. *Development* 138: 2987-98.

24. Jouvin-Marche E, Attuil-Audenis V, Aude-Garcia C, Rachidi W, Zabel M, Podevin-Dimster V, Siret C, Huber C, Martinic M, Riondel J, Villiers CL, Favier A, Naquet P, Cesbron JY, Marche PN. Overexpression of cellular prion protein induces an antioxidant environment altering T cell development in the thymus. *J Immunol* 176: 3490-3497, 2006.

25. Kingdom JC, Kaufmann P. Oxygen and placental vascular development. *Adv Exp Med Biol* 474: 259-75, 1999.

26. Klamt F, Dal-Pizzol F, Conte da Frota ML, Jr., Walz R, Andrades ME, da Silva EG, Brentani RR, Izquierdo I, Fonseca Moreira JC. Imbalance of antioxidant defense in mice lacking cellular prion protein. *Free Radic Biol Med* 30: 1137-44, 2001.

27. Krachler M, Rossipal E, Micetic-Turk D. Trace element transfer from the mother to the newborn--investigations on triplets of colostrum, maternal and umbilical cord sera. *Eur J Clin Nutr* 53: 486-94, 1999.

28. Liang J, Bai F, Luo G, Wang J, Liu J, Ge F, Pan Y, Yao L, Du R, Li X, Fan R, Zhang H, Guo X, Wu K, Fan D. Hypoxia induced overexpression of PrP(C) in gastric cancer cell lines. *Cancer Biol Ther* 6: 769-74, 2007.

29. Lowndes SA, Sheldon HV, Cai S, Taylor JM, Harris AL. Copper chelator ATN-224 inhibits endothelial function by multiple mechanisms. *Microvasc Res* 77: 314-26, 2009.

30. Martelli, A., et al. 2007. Folding and turnover of human iron regulatory protein 1 depend on its subcellular localization. *Febs J* 274:1083-1092.

31. McLennan NF, Brennan PM, McNeill A, Davies I, Fotheringham A, Rennison KA, Ritchie D, Brannan F, Head MW, Ironside JW, Williams A, Bell JE. Prion protein accumulation and neuroprotection in hypoxic brain damage. *Am J Pathol* 165: 227-35, 2004.

32. Moser M, Colello RJ, Pott U, Oesch B. Developmental expression of the prion protein gene in glial cells. *Neuron* 14: 509-17, 1995.

33. Myatt L. Role of placenta in preeclampsia. *Endocrine* 19: 103-11, 2002.

34. Pantopoulos, K., et al. 1997. Differences in the regulation of iron regulatory protein-1 (IRP-1) by extra- and intracellular oxidative stress. *J Biol Chem* 272:9802-9808.

35. Prusiner SB. Prions. *Proc Natl Acad Sci U S A* 95: 13363-83, 1998.

36. Raj T, Kanellakis P, Pomilio G, Jennings G, Bobik A, Agrotis A. Inhibition of fibroblast growth factor receptor signaling attenuates atherosclerosis in apolipoprotein E-deficient mice. *Arterioscler Thromb Vasc Biol* 26: 1845-51, 2006.

37. Ranjkesh F, Jaliseh HK, Abutorabi S. Monitoring the Copper Content of Serum and Urine in Pregnancies Complicated by Preeclampsia. *Biol Trace Elem Res.* 144: 58-62, 2011.

38. Saryan LA, Mailer K, Krishnamurti C, Antholine W, Petering DH. Interaction of 2-formylpyridine thiosemicarbazonato copper (II) with Ehrlich ascites tumor cells. *Biochem Pharmacol* 30: 1595-604, 1981.

39. Taraboulos A, Raeber AJ, Borchelt DR, Serban D, Prusiner SB. Synthesis and trafficking of prion proteins in cultured cells. *Mol Biol Cell* 3: 851-63, 1992.

40. Thackray AM, Bujdoso R. Elevated PrP^{C} expression predisposes to increased HSV-1 pathogenicity. *Antivir Chem Chemother* 17: 41-52, 2006.

41. Weissmann C, Fischer M, Raeber A, Bueler H, Sailer A, Shmerling D, Rulicke T, Brandner S, Aguzzi A. The role of PrP in pathogenesis of experimental scrapie. *Cold Spring Harb Symp Quant Biol* 61: 511-22, 1996.

42. Xie H, Kang YJ. Role of copper in angiogenesis and its medicinal implications. *Curr Med Chem* 16: 1304-14, 2009.

Figure legends

Figure 1

Expression and characterization of PrP^C protein in human placenta.

(**A**) Immunolocalization of PrP^C using monoclonal antibody (mAb) anti-PrP (3F4) in chorionic villi (**a**) and placental column (**b**) at 10 wg. (**c)** and **(d)** represent negative controls. Stars in panels (**a**) and (**b**) show the strongest sites of PrP^C immunoreactivity. Cytotrophoblast (Ct), Hobfauer cells (Ho), Extravillous trophoblast (EVT), syncytiotrophoblast (St) and blood vessels (Bv). (**B**) RT-PCR detection of PrP^C mRNA in HTR and BHK cells stably expressing or not PrP^C protein. (**C**) Steady-state expression of PrP^C in HTR and BHK cells. Equal amounts of proteins extract from HTR and BHK cells stably expressing or not PrP^C protein were separated by 12% SDS–PAGE, transferred to nitrocellulose and immunoblotted with anti-PrP (3F4). The high- (H), intermediate- (I), and unglycosylated (U) forms are indicated, respectively, by black, white, and gray arrowheads. (**D**) Endoglycosidase H (H) and N-glycosidase F (F) digestions. (**E**) Immunofluorescence localization of PrP^C proteins in non-permeabilized (a) and Triton-permeabilized HTR cells (b). HTR cells were fixed and visualized by indirect immunofluorescence using anti-PrP (3F4) and fluorescein-conjugated goat anti-mouse Ab. Pictures were obtained with the LSM 510 imaging system using a 63/1.4 objective. Bar, 10 µm.

Figure 2

Copper treatment increases PrP^C expression in HTR cells.

(**A**) Protein levels of PrP^C after exposure of HTR cells to Cu. HTR cells were incubated with 100 µM of copper sulfate for the indicated time and cell lysates were subjected to immunoblots using anti-PrP (3F4) or anti-Na^+/K^+-ATPase antibody. The high- (H), intermediate- (I), and unglycosylated (U) forms are indicated, respectively, by black, white, and gray arrowheads. (**B**) The expression levels of PrP^C mRNAs, following treatment with 100 µM of Cu were quantified by real-time RT-PCR, normalized to the 18S rRNA levels and plotted as function of incubation time (h). Data are expressed as mean ± SE (n=6). Values overwritten with stars are significantly different from the control (0h) ($P < 0.05$).

(**C**) Detection of biotinylated PrP^C protein in HTR cells extract before (lysaste; lys) and after Cu stimulation for the indicated time. PrP^C was covalently labelled with NHS-SS-biotin at 4 ℃. Biotinylated (biot) PrP^C was affinity–isolated on streptavidin (strep) beads and immunoblotted with anti-PrP mAb (3F4). Neither intermediate- (I, white arrowheads) nor unglycosylated (U, gray arrowheads) forms were susceptible to biotinylation.

(**D**) Biotinylated high-glycosylated form of PrP^C quantified using Image J was plotted as function of incubation time (h). Data are expressed as mean ± SE (n=3). Values with asterisk are significantly different from the control (0h) ($P < 0.05$).

Figure 3

Depletion of PrP^C in HTR cells enhances Cu-induced ROS accumulation, increases cell Cu content and causes acute cell death.

Data are expressed as mean ± SE (n=6). Values with an asterisk are significantly different from the corresponding control ($P < 0.05$).

(**A**) PrP^C reduces the accumulation of the Cu-induced ROS. HTR or PrP-knockdown HTR cells (PrP^C (-)) were incubated with 50 µM DCFH-DA for 45 min. After wash, cells were then incubated with vehicle (control), 50 or 100 µM Cu at 37 ℃ for 2h. After washing, the DCF fluorescence was determined at an excitation of 485 nm and emission of 538 nm by a microplate reader.

(**B**) Determination of the catalase activity in wt and knockdown-PrP^C HTR cells under the same conditions described in 3A in the presence of 100 µM of Cu.
(**C**) ICP-AES determination of Cu content in HTR cells under basal and following 24h stimulation with Cu of wt and PrP^C depleted HTR cells (PrP^C (-)).
(D) PrP^C reduces cell death caused by Cu. HTR (*solid circles*) or PrP-knockdown HTR cells (PrP^C (-)) (*open circles*) were incubated without (*solid triangles*) or with 100 µM Cu (*open triangles*) for indicated time. Cells were trypsinized and harvested. Dead cells were determined by trypan blue staining.

Figure 4
PrP^C modulates the effect of Cu on HTR tube-like formation.
(**A**) Photographs of wt and PrP^C depleted HTR cells (PrP^C (-)) cultured on matrigel following Cu stimulation (100 µM) at the indicated time. FGF2 (20 ng/ml) was used as positive control.
(**B**) Quantification of the number of tube like structures formed after 24h using Metamorph software. Data are expressed as mean ± SE (n=4). Values with different letters are significantly different from each other ($P < 0.05$).

Figure 5
PrP^C modulates the effect of Cu on the migration and proliferation of HTR cells.
(**A**) Photographs of wt and PrP^C depleted HTR cells monolayer (PrP^C (-)) at 0h and 24h after their wounding and following their stimulation by Cu at 50 or 100 µM. (**B**) Percentage of wound closure 24h after the treatments with Cu. (*$P<0.05$). Data are expressed as mean ± SE (n=4). Values with an asterisk are significantly different from the corresponding control ($P < 0.05$). (**C**) Proliferation of wt and depleted PrP^C HTR cells are reported as percentage of the indicated control. Cells were trypsinized, harvested, and counted using a cell counter. Data are expressed as mean ± SE (n=4). Values with an asterisk are significantly different from the corresponding control ($P < 0.05$)

Figure 6
Overexpression of PrP^C in HTR cells induces ROS accumulation, causes cell death, and affects cell proliferation and migration.
(**A,B**) Transiently transfected HTR cells with mock (-) or EGFP-hPrP (+) plasmid construct were solubilized and equal amounts of proteins were separated by 12% SDS–PAGE. Proteins were transferred to nitrocellulose and immunoblotted with anti-PrP3F4 (**A**) and anti-GFP (**B**) antibodies. EGFP–$hPrP^C$ fusion protein was not detected in non-transfected HTR cells (**B**). The molecular weight of the chimera protein (~60 kDa) corresponded to the addition of the EGFP tag (~27 kDa) to PrP^C (~33 kDa). The high- (H), intermediate- (I), and unglycosylated (U) forms are indicated, respectively, by black, white, and grey arrowheads.
(**C**) Effect of PrP^C overexpression on HTR cells proliferation and viability.
(**D**) PrP^C overexpression increases ROS production that was attenuated by addition of Cu. HTR or PrP^C-overexpressing HTR cells (PrP^C ++) were incubated with 50 µM DCFH-DA for 45 min. After wash, cells were then incubated with vehicle (control) or 5 µM Cu at 37 °C for 2h. After washing, the DCF fluorescence was determined at an excitation of 485 nm and emission of 538 nm in a microplate reader.
(**E**) Representative photographs of HTR cells migration in control and PrP^C transfected cells at the indicated time. Migration was assessed in the absence and presence of 5 µM of Cu.
(**F**) Percentage of wound closure HTR cells in the presence and absence of 5 µM of Cu for the indicated time. Data are expressed as mean ± SE (n=4). Values with an asterisk are significantly different from the corresponding control ($P < 0.05$).

Figure 7

Determination of circulating Cu levels, litter sizes, and placental efficiency in wild type (wt), Tga20 and PrP-/- mice.

(**A**) Effect of Cu supplementation on blood Cu concentration, determined by ICP-AES, in wt, Tga20 and PrP-/- mice in the absence or presence of Cu supplementation. Data are expressed as mean ± SE (n=4). Values with an asterisk are significantly different from the corresponding control ($P < 0.05$).

(**B**) The litter size was examined in wt, Tga20 and PrP-/- mice under conditions described in 7A. Data represent the mean number of pups counted after the sacrifice of gravid mice (n=45) at E10.5, E14.5 and E17.5.

Values with an asterisk are significantly different from the corresponding control ($P < 0.05$).

(**C**) Fetal (a, b), placental weights (c, d), and placental efficiency (e, f) of wt, Tga20 and PrP-/- Pups were collected at E14.5 and E17.5 under conditions described in 7A. Placental efficiency is determined as ratio of fetal to placental weight). Data are presented as a box plot (* $P < 0.05$, by ANOVA followed by Dunn's Method).

Figure 8

PrP^C expression level influence placental expression profile of CD31 protein and Mash2, proliferin, GCm1 and CD31 transcript.

(**A**) Immunodetection of CD31, a marker of endothelial cells, in the labyrinth (L) zone of placentas collected from wt, Tga20 and PrP-/- mice at E14.5.

(**B**) Representative immunoblot of CD31 protein in placentas from wt, Tga20 and the PrP-/- control and Cu-treated mice at E14.5. β-actin was used to standardize for loading.

(**C**) Image J quantification of the expression levels of the CD31 protein in placentas of wt, Tga20 and PrP-/- mice, at E14.5, under conditions described in (**6B**). Data are expressed as mean ± SE (n=4). Values with an asterisk are significantly different from the corresponding control ($P < 0.05$).

(**D**) Expression of Mash2, proliferin, GCm1 and CD31 mRNAs were quantified by real-time RT-PCR, normalized to the GAPDH mRNA levels, and plotted as function of day post co ïome (dpc; 10.5, 14.5, and 17.5). Transcript was isolated from whole placentas of normal and Cu-treated wt, Tga20 and PrP-/- mice. Data are presented as the mean + SEM of triplicates. (*$P < 0.05$, by ANOVA followed by Dunn's Method).

Figure 9

HIF-1α expression in the placenta of Tga20 and PrP-/- mice.

(**A**) Representative immunoblot of HIF1α expression in the placenta of the normal and Cu-treated wt, Tga20 and PrP-/- mice at E10.5 and E14.5. β-actin was used to standardize for loading.

(**B**) Image J quantification of the expression levels of HIF1α protein standardized to β-actin expression in placentas of wt, Tga20 and PrP-/- mice, at E10.5 and E14.5, under conditions described in (**11A**). Data are expressed as mean ± SE (n=4). Values are significantly different from the corresponding control ($P < 0.05$). A.U corresponds to arbitrary unit.

Figure 1

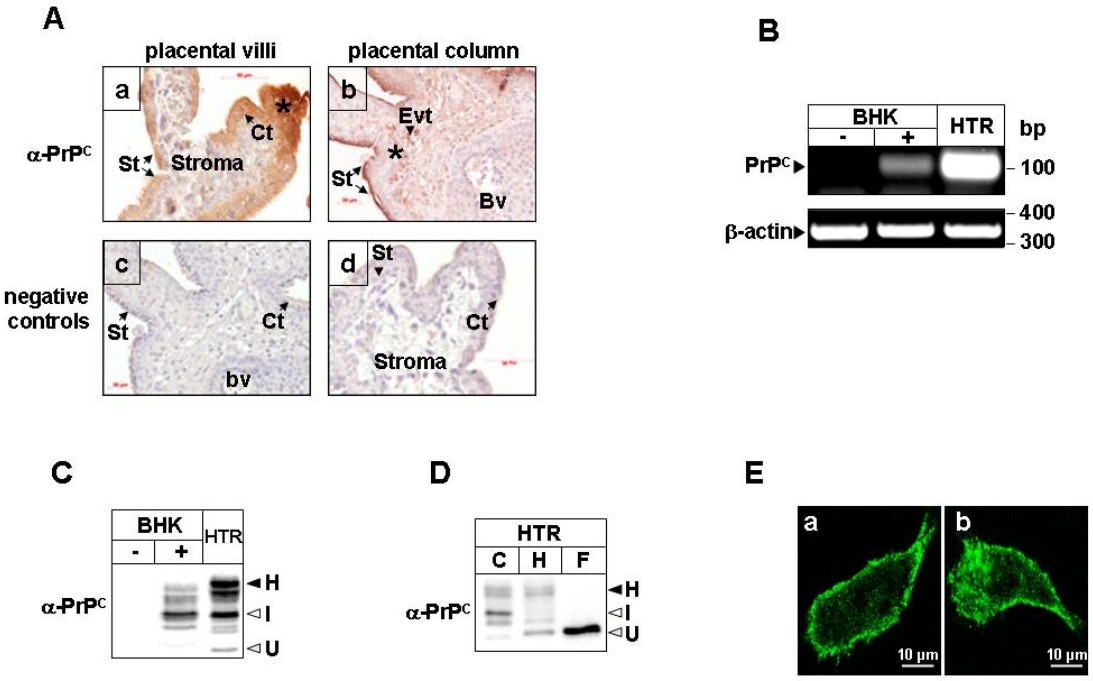

Figure 2

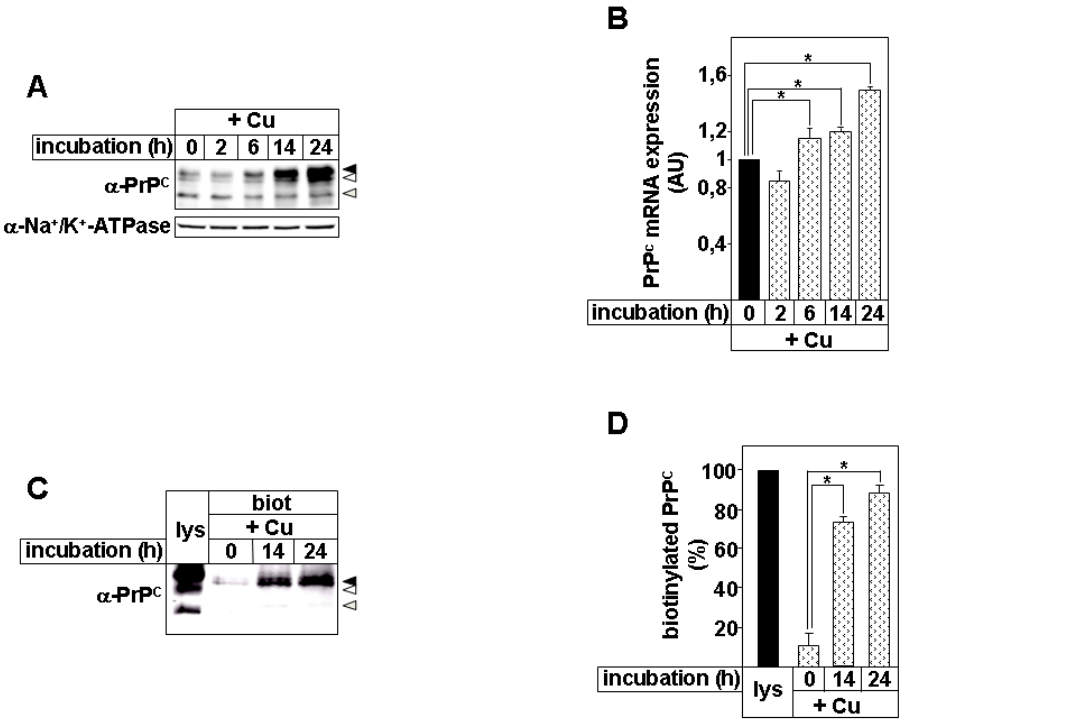

Figure 3

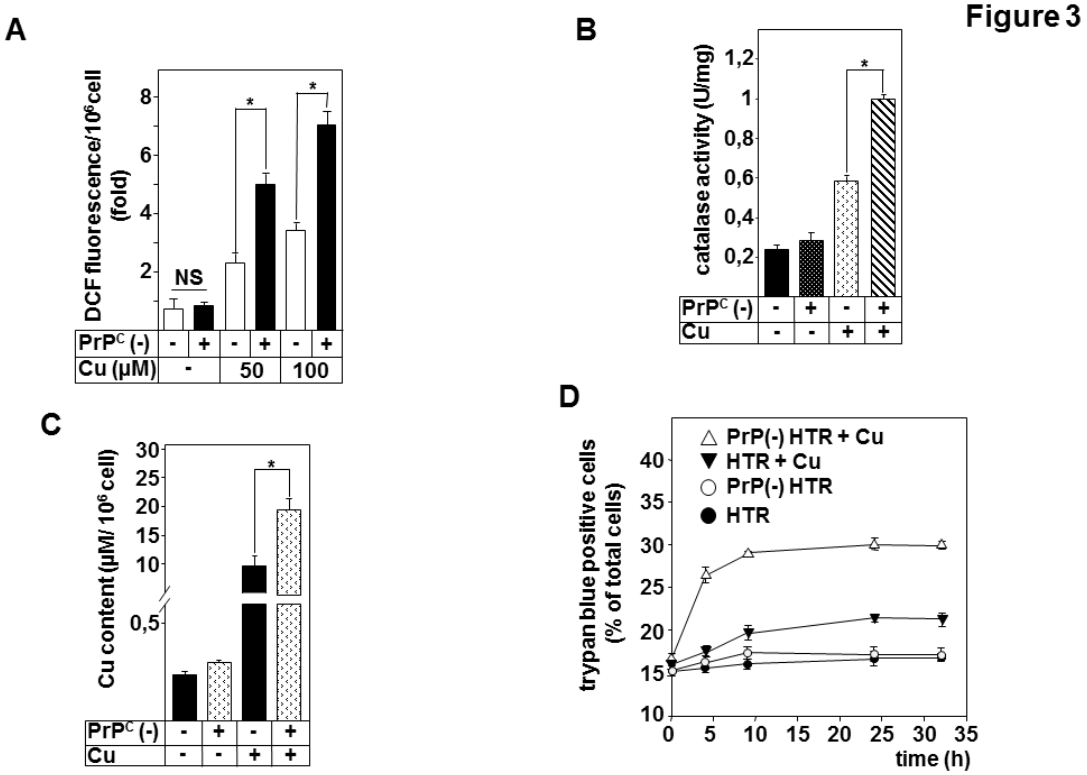

Figure 4

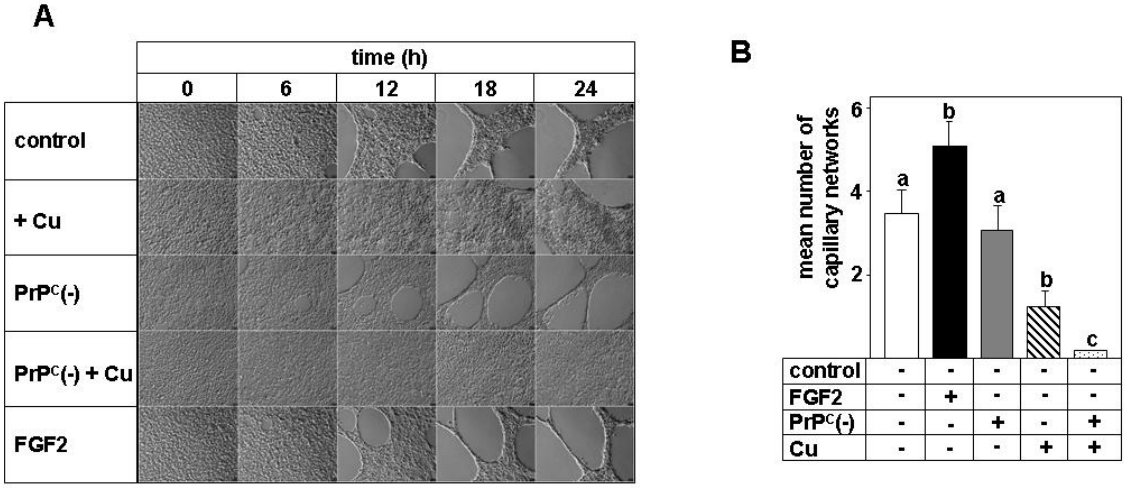

Figure 6

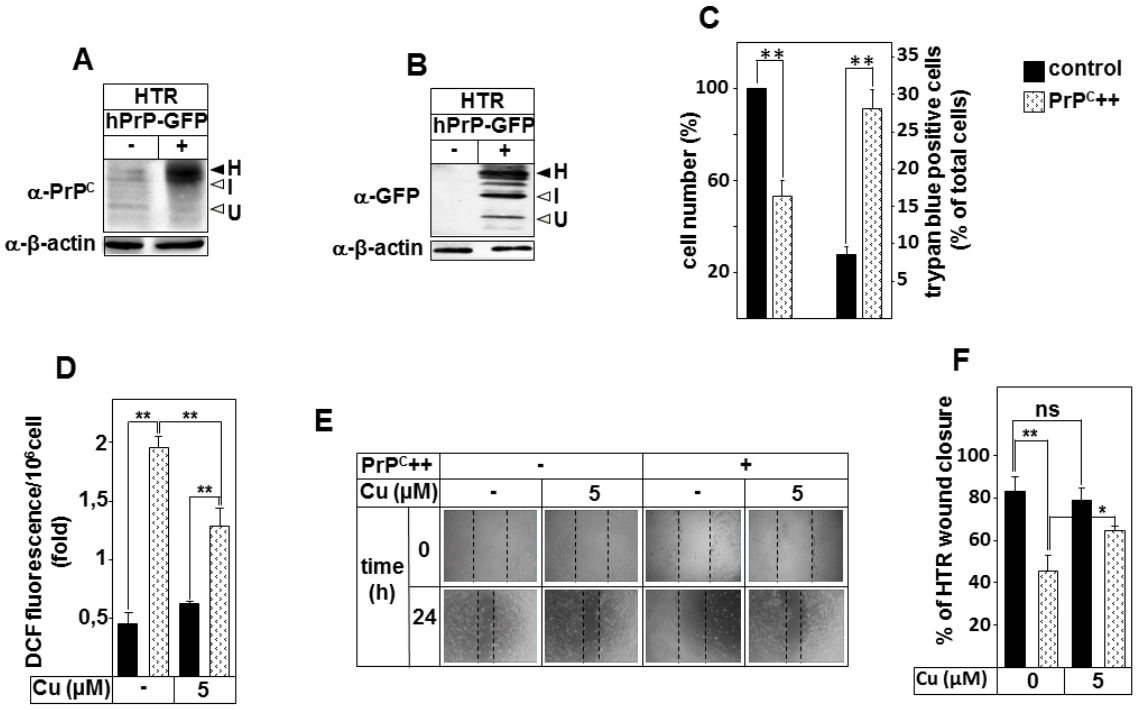

Figure 5

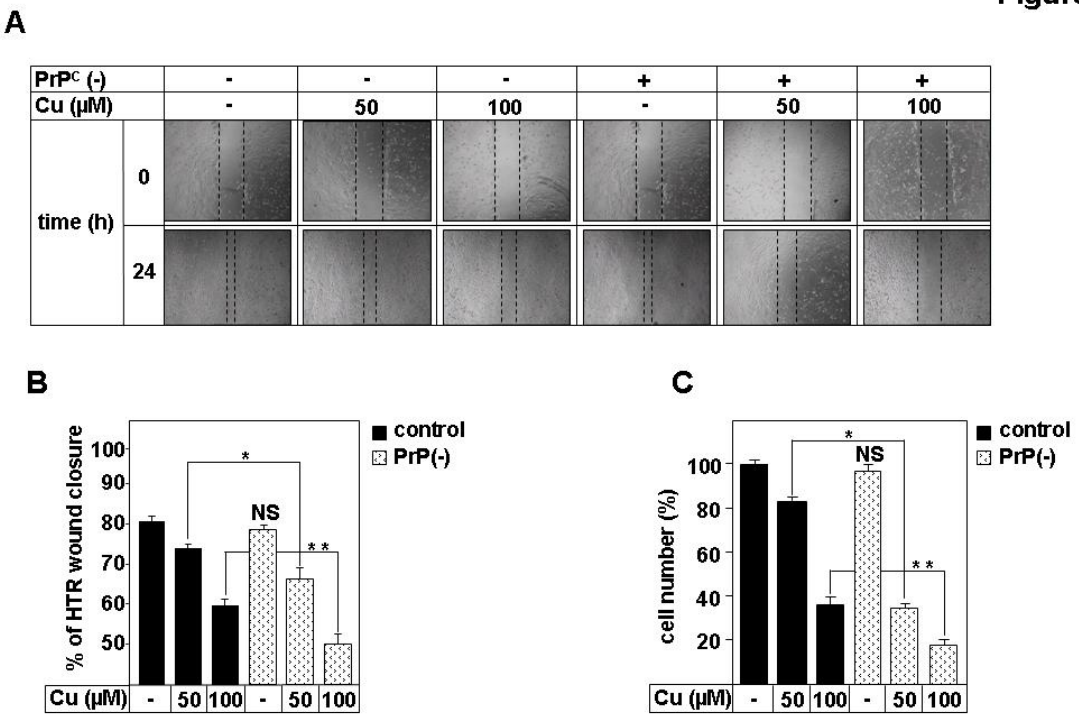

Figure 7

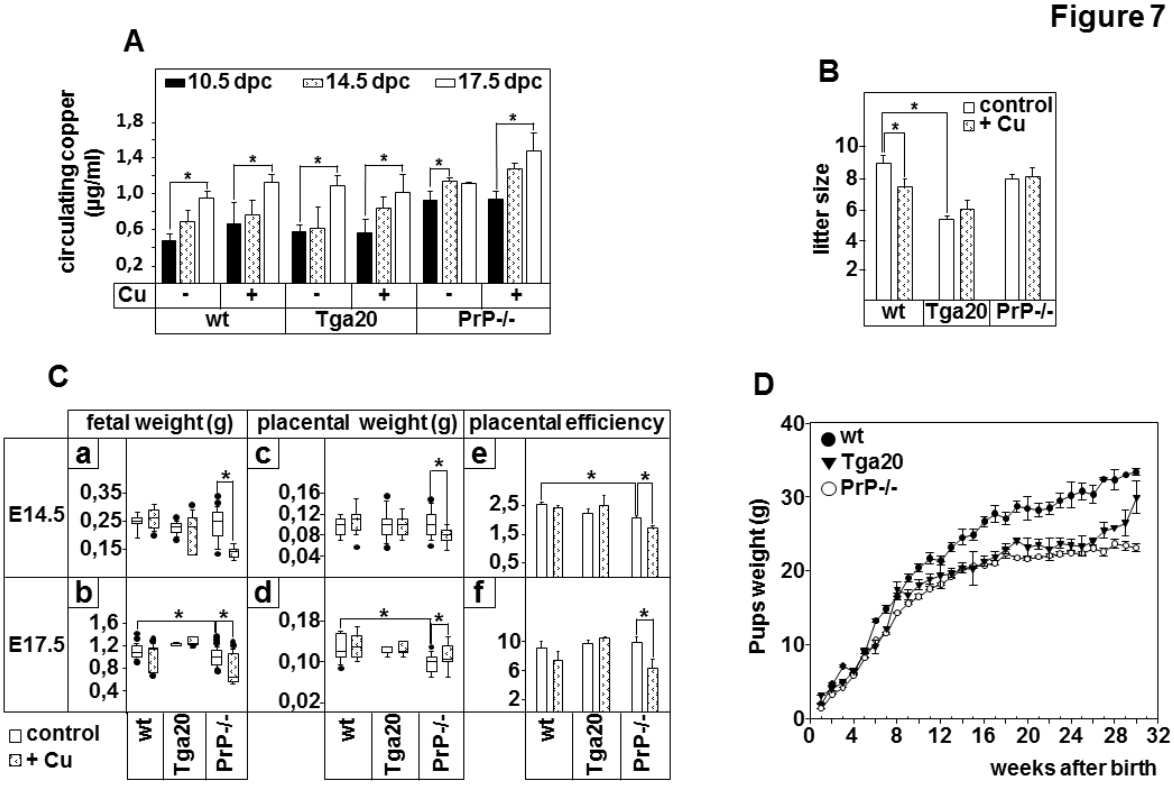

Figure 8

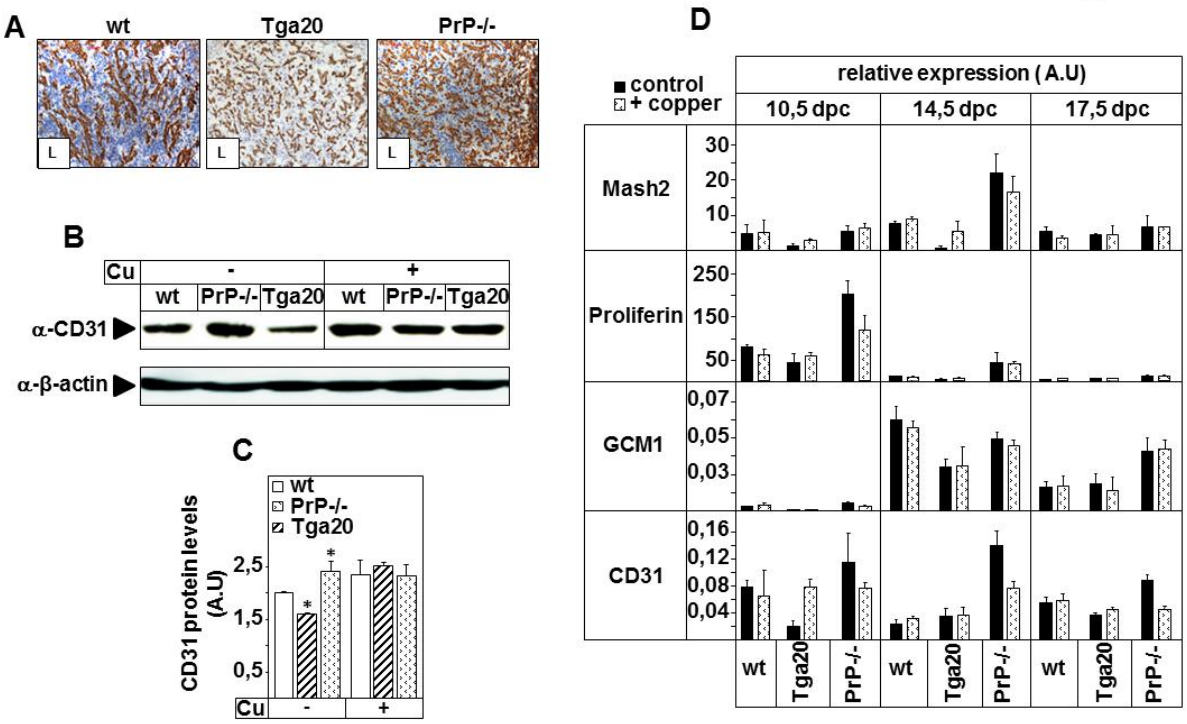

Figure 9

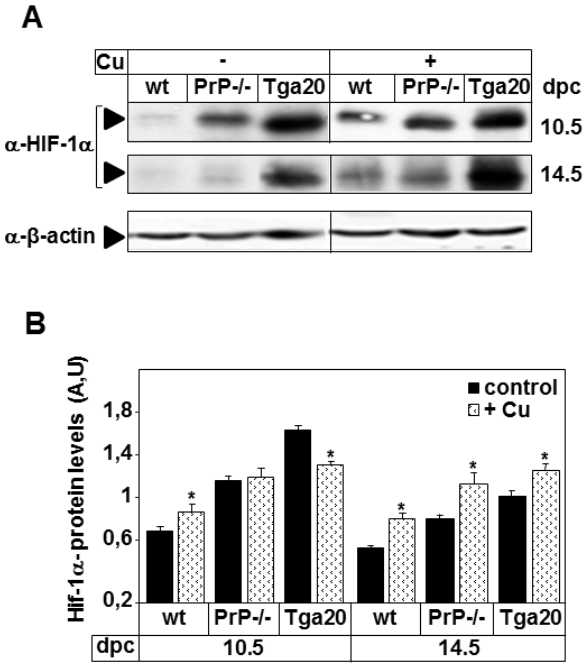

Figure S1

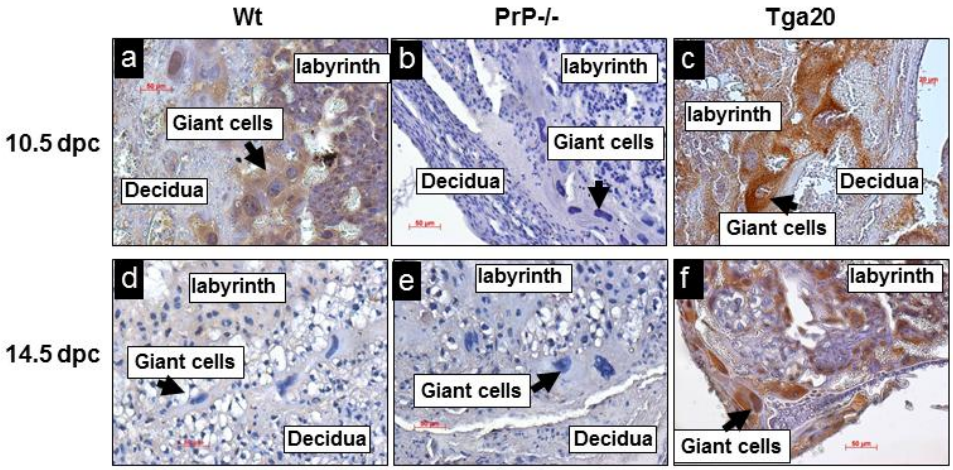

Figure S2

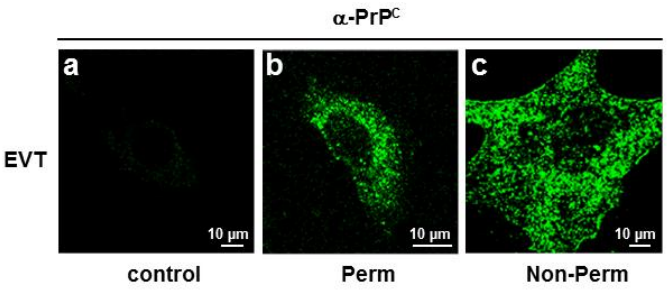

Figure S3

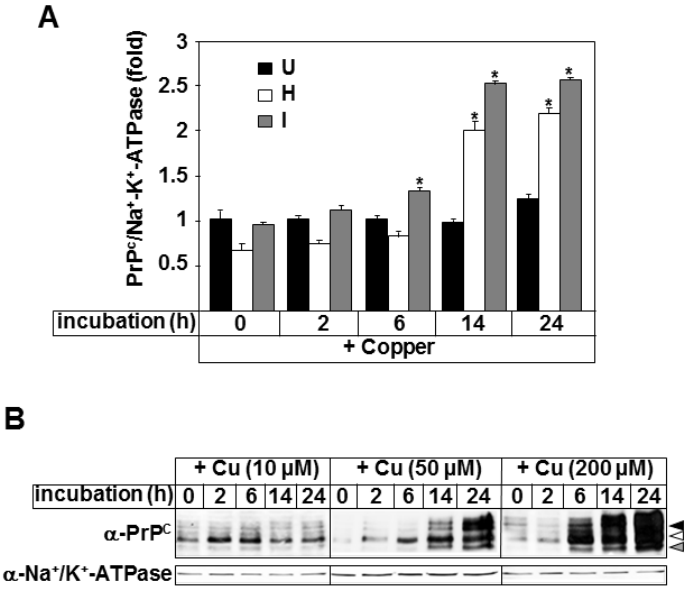

Figure S4

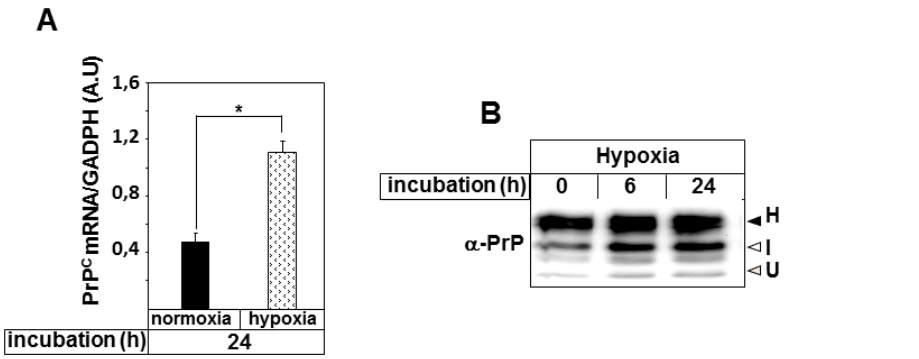

Figure S5

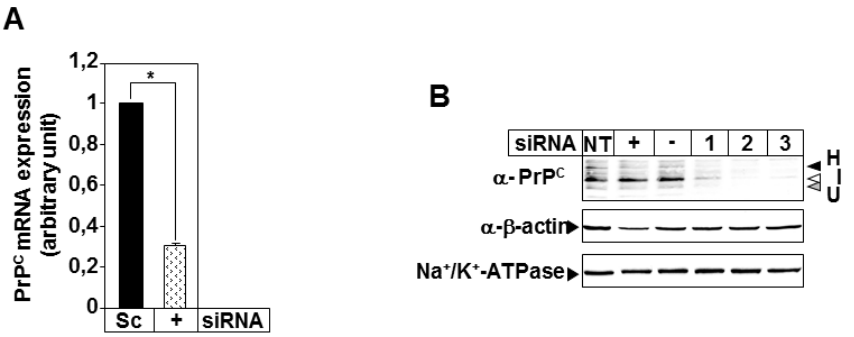

Figure S6

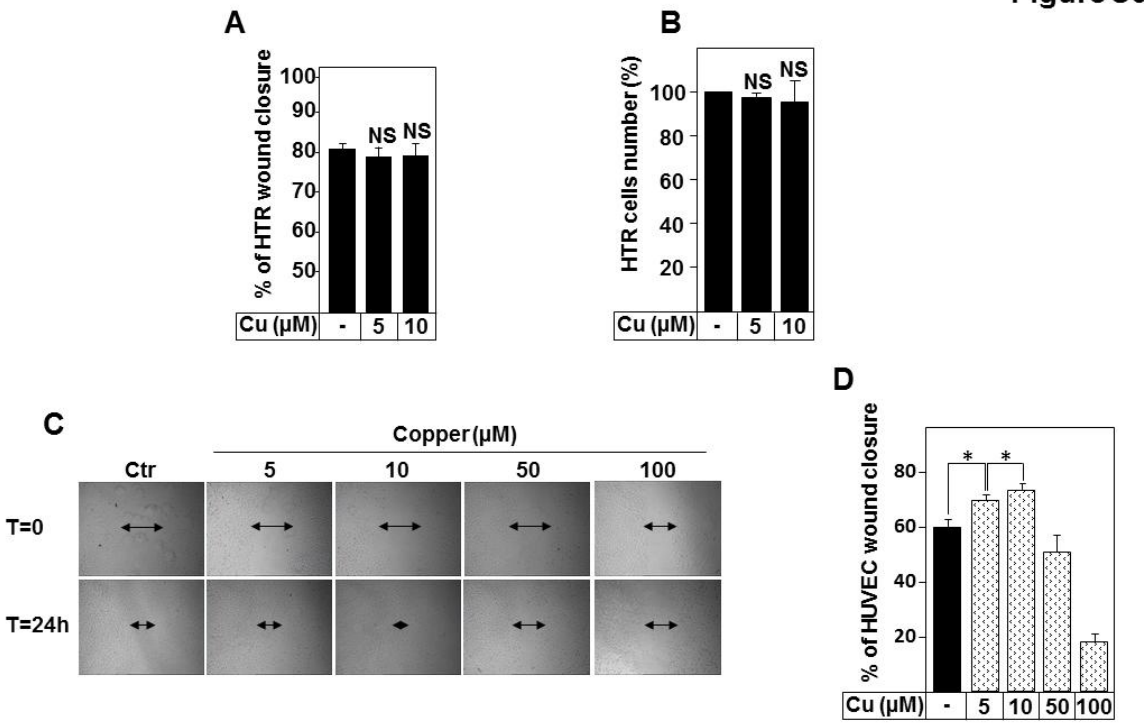

Figure S7

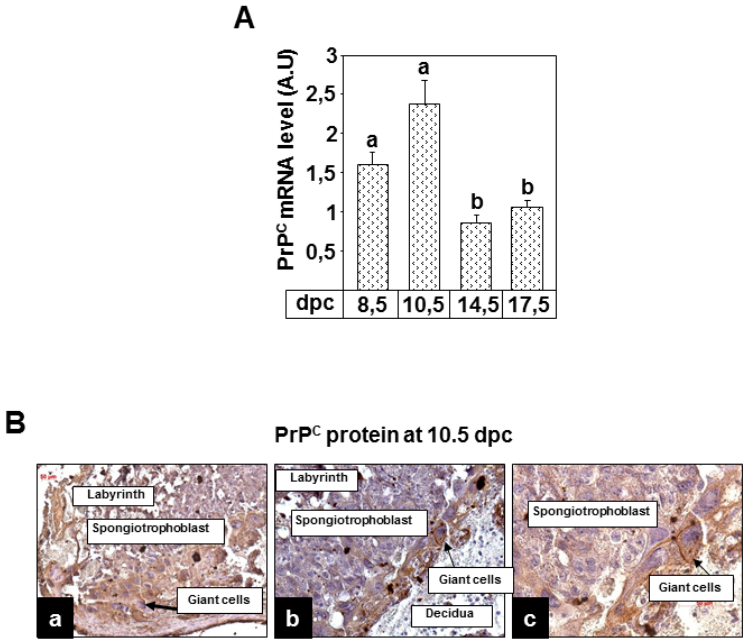

Figure S8

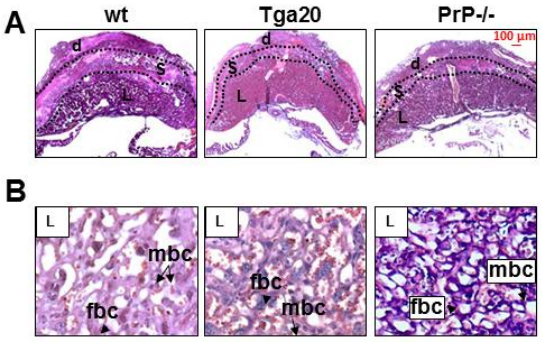

Figure S9

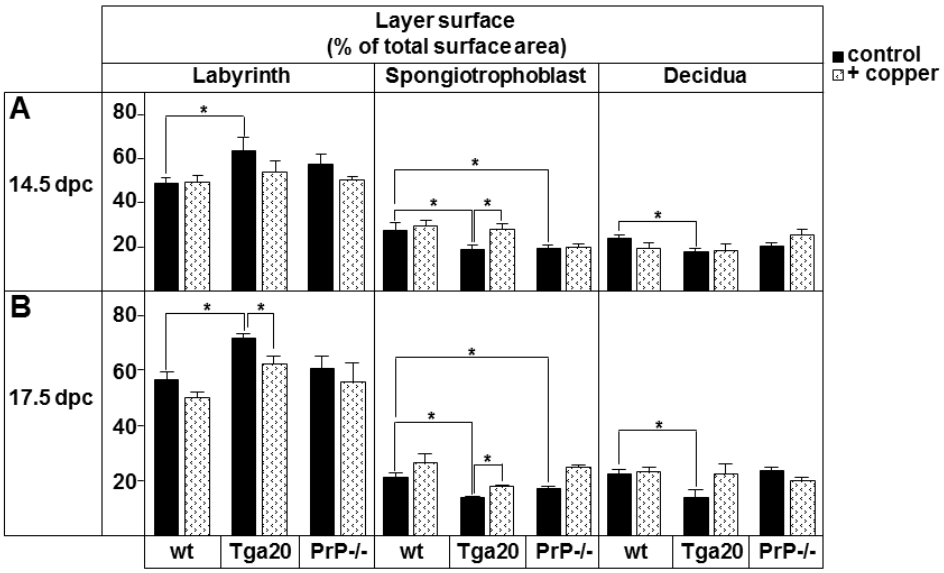

Supplemental Experimental Procedures, Legends and Tables:

Supplemental Experimental Procedures

Immunohistochemistry

Immunohistochemistry was performed as described previously (16). For antigen detection, sections were incubated with the following antibodies; anti-PrP^C (3F4, Millipore, France) and anti-CD31 (DAKO, France). Immunopositive staining was detected using a Vectastain ABC kit (Vector Labs), using DAB as the chromogen (Vector Labs). Slides were counterstained using hematoxylin and eosin (H&E) (Sigma Aldrich, France).

Isolation of primary cytotrophoblast and cell culture

Placental cytotrophoblasts (CT) isolated from first-trimester human placentas (10-12 wk of gestation, n =6) and trophoblast-derived HTR-8/SVneo cells, kindly provided by Dr. Charles H. Graham (Queen's University, Kingston, ON, Canada), were cultured as previously reported (21). BHK-21 cells (CCL-10; (ATCC)), stably expressing hemaglutinin (HA) N-terminal tagged human PrP^C, were cultured as previously described (15). Where indicated, cells were treated with vehicle or different concentrations of copper for the corresponding time. For hypoxic conditions, CT and HTR cells were cultured under 3% O_2, 92% N_2 and 5% CO_2) for the indicated time.

siRNA knockdown of PrP^C and Transfection

The siRNA oligonucleotides duplexes (Ambion, Austin, TX, USA) specific for human PrP^C were purchased from Ambion. The siRNA sequences (5-CAGCAAATAACCATTGGTTAA-3) to inhibit PrP^C mRNA synthesis had dTdT overhanging at their 21 terminus. Control siRNA, which is a pool of several control siRNAs, was purchased from Ambion. Transfection of siRNA was carried out using Silencer siRNA Transfection II Kit (Ambion, Austin, TX, USA). Transfections were performed for 72 h, and the transfected cells were washed, and their mRNA or proteins were extracted and subjected respectively to real-time RT-PCR or Western blot analysis (21).

Cell wound-healing assay

To evaluate the HTR migration capacity, wound healing assays were performed, on the normal and PrP^C siRNA knockdown HTR cells, as previously reported (6). The width of denuded area was measured using an electronic grid and the distances crossed by cells were determined using Scion Image software (version 4.0.2; Scion Corp). Results were expressed as percent of control (initial wound).

Cell proliferation

Cell proliferation of normal and PrP^C siRNA knockdown HTR cells was determined on days 0 and 3 by hemocytometer analysis of a trypsinized aliquot of cells (6). Results of at least three separate experiments were expressed as percent of control.

Tube-like formation assay

Tube formation was assayed as previously described (21). In brief, normal and PrP^C siRNA knockdown HTR cells were seeded, allowed to settle for 4h before the treatment, and then placed inside a video microscopy platform. Time lapse of Z series images were collected and controlled by MetaMorph software (Universal Imaging, Downingtown, PA). For each Z series images, the best focus was chosen before the reconstitution of the movie. At least 12 fields were examined per well and each experimental condition was tested in triplicate.

Immunofluorescence microscopy

Plasma membrane and intracellular expression of PrP^C in non-pemeabilized and Triton X-100 permeabilized HTR cells, respectively, were visualized using monoclonal anti-PrP (3F4, Millipore, France), and fluorescein- or rhodamine-conjugated goat anti-mouse antibodies (Jackson ImmunoResearch Laboratories).

For plasma membrane expression, PrP^C protein was co-localized with biotinylated cell surface proteins using monoclonal anti-biotin and fluorescein-conjugated goat anti-mouse antibodies (Jackson ImmunoResearch Laboratories). Fluorescence micrographs were obtained with a Zeiss LSM 510 laser confocal fluorescence microscope as previously described (15).

Electrophoresis and immunoblotting

Whole-cell samples prepared as previously described (16) were subjected to a SDS-PAGE (12%) and immunoblot analysis using mouse monoclonal anti-PrP (3F4, Millipore, France), anti-Na+/K+-ATPase (Hybridoma Bank, University of Iowa, Iowa), anti-HIF-1α (France), and ECL (Amersham Biosciences). Images were captured by using the Molecular Imaging acquisition system (Vilber Lourmat, France).

Endoglycosidase digestion

To distinguish between high mannose and complex-type N-linked oligosaccharide modification of PrP^C, cell lysates were incubated with endoglycosidase H (H) and peptide N-glycosidase F (F) as previously reported (15). The mobility shift of deglycosylated PrP^C was visualized by immunoblotting using anti-PrP mAb.

Cell surface biotinylation

To determine the cell surface expression of PrP^C protein, HTR cells were selectively biotinylated as described previously (15). Biotinylated PrP^C protein was isolated by immunoprecipitation on Streptavidin–Sepharose (Sigma–Aldrich) and visualized by immunobloting using anti-PrP mAb. The amount of biotinylated PrP^C relative to the control (time (t) = 0) was quantified by scanning the gel lanes followed by analysis with the Scion Image program (http://www. scioncorp.com/pages).

RNA isolation and Reverse Transcriptase Polymerase Chain Reaction Analysis

Total RNA was extracted from HTR cells and mice tissues samples using a rapid RNA isolation system (Qiagen RNeasy, Courtaboeuf, France). Reverse transcription was performed on 1μg total RNA with Superscript II-RnaseH reverse transcriptase (Invitrogen, Cergy Pontoise, France) under conditions recommended by the manufacturer.

Real-Time Polymerase Chain Reaction analysis

Prion, GCM1, Mash2, proliferin, CD31, GAPDH mRNAs, and 18S rRNA expression were quantified by real-time RT-PCR using a Light Cycler apparatus (Roche Diagnostics, Meylan, France). The PCR was performed using the primers shown in Table S1 (see supplementary data) and SYBR green PCR core reagents (Light Cycler-FastStart Master SYBR Green I, Roche Diagnostics). The results were normalized to 18S rRNA and/or GAPDH mRNA expression levels. To assess linearity and efficiency of PCR amplification, standard curves for all transcripts were generated by using serial dilutions of cDNA. The RealQuant analysis software (Roche Diagnostics) was used to quantify relative levels of expression.

Intracellular copper determination

To evaluate the intracellular copper concentration, HTR cells, serum, and tissue samples (maternal liver and placenta) from C57, PrP-/- and Tga20 mice were collected and stored at -80°C. Samples were vacuum-dried and mineralized in 70% nitric acid before analysis with Inductively Coupled Plasma-Atomic Emission Spectrometry (ICP-AES) with a Varian, Vista MPX instrument (30). The copper content was reported relatively to the number of HTR cells, to the serum volume, and to the weight of the tissue samples, respectively.

ROS Measurements

Normal and PrP^C siRNA knockdown HTR cells (1×10^6 cells/well) were seeded in a 24-well plate and cultured for 24 h. The cells were washed and changed to serum-free media and incubated with 50 μM 5-(and 6)-chloromethyl-2′,7′-dichlorodihydrofluorescein diacetate acetyl ester (H_2DCFDA; Invitrogen) for 45 min. The conversion of H_2DCFDA to fluorescent DCF was measured using a plate reader Infinite M200 (TECAN, France) (34).

Catalase enzyme activity assays

Normal and PrP^C siRNA knockdown HTR cells were used to determine catalase enzyme activity. Catalase activity was determined spectrophotometrically at 240 nm by measuring the decomposition of hydrogen peroxide by the method of Beers and Sizer (3).

Figures Legends and Tables

Figure S1:
PrP^C protein in wt, PrP-/- and Tga20 mice placentas.
(a), (b) and (c) show PrP^C expression in placentas at 10.5 dpc. (d), (e) and (f) show PrP^C expression in placentas at 14.5 dpc. Note that PrP^C protein is absent from the PrP-/- placentas at both terms. In wt placentas, PrP^C expression is strong at 10.5 dpc with a significant decrease at 14.5 dpc. In Tga20 PrP^C expression is very strong at 10.5 dpc with a total maintenance of expression at 14.5 dpc. Arrows indicate giant cells that showed a high expression level of PrP^C. Scale bar is 50 µm.

Figure S2:
Expression of PrP^C in extravillous trophoblast cells.
Indirect immunoflorescence was performed to determine the cellular expression and localization of PrP^C protein in non-premeabilized (**c**) and permeabilized (**b**) primary isolated extravillous trophoblast (EVT) cells from first trimester human placenta. EVT cells were fixed and PrP^C protein visualized using anti-PrP (3F4) and fluorescein-conjugated goat anti-mouse Ab. Pictures were obtained with LSM 510 imaging system using a 63/1.4 objective. Bar, 10 µm.

Figure S3:
Dose response and time course effects of copper on PrP^C expression in HTR cells.
(**A**) Image J quantification of the expression levels of the different forms (I, H and U) of PrP^C protein standardized to Na^+/K^+-ATPase expression in HTR cells treated with 100 µM of Cu for the indicated time. Data are expressed as mean ± SE (n=4). Values with asterisk are significantly different from the corresponding control ($P < 0.05$). (**B**) Effects of different Cu concentration (10, 50, and 200 µM) on PrP^C expression in HTR cells. Copper treatments were performed as described in materiel and methods and PrP^C detection was determined using immunoblot with anti-PrP (3F4).

Figure S4:
Placental hypoxia stimulates PrP^C expression.
HTR cells were treated with 100 µM of Cu for the indicated time and mRNA or protein extract were prepared as described in materiel and methods. (**A**) Expression of PrP^C mRNAs were quantified by real-time RT-PCR, normalized to the GAPDH mRNA levels. Data are presented as the mean + SEM (n=4). Values with an asterisk are significantly different from the corresponding control ($P < 0.05$). (**B**) Representative immunoblot of PrP^C expression in HTR cells cultured under 3% oxygen tension for the indicated time.

Figure S5:
Effect of siRNA treatment on PrP^C expression in HTR cells.
Cells were analysed for the loss of PrP^C mRNA and protein expression 48 h after transfection using real-time RT-PCR (**A)** and immunoblotting **(B)**, respectively. 1, 2 and 3 designate three

different siRNA used to silence PrP^C mRNA. Scrambled siRNA (Sc) served as non-specific control siRNAs. *P<0.05. (H) for the hyper-, (I) for the intermediate-, and (U) for the unglygosylated form.

Figure S6:
Effect of Cu on HTR and HUVEC cells proliferation and migration.
(**A,B**) Percentage of wound closure and number of HTR cells 24h following Cu treatments (5 and 10 μM).
(**C**) Representative photographs of HUVEC monolayers at 0 and 24h after their wounding under the following conditions: control (Ctr), and in the presence of Cu (5, 10, 50 and 100 μM). (**D**) Percentage of wound closure 24h after Cu treatments. All Data are expressed as mean ± SE (n=4). Values with an asterisk are significantly different from the corresponding control ($P < 0.05$), NS; non-significant.

Figure S7:
Placental PrP^C mRNA and protein expression throughout mouse gestation.
(**A**) Expression of PrP^C mRNAs was quantified by real-time RT-PCR, normalized to the GAPDH mRNA levels and plotted as function of gestational age (days post co ïome; 8.5, 10.5, 14.5, and 17.5). Data are expressed as mean ± SE (n=6). Values with different superscripts are significantly different from each other ($P < 0.05$). (**B**) Immunolocalization of PrP^C in C57 wt mice placentas. (b) and (c) correspond to successive magnifications of photograph (a).

Figure S8:
Placentation defect in Tga20 and PrP-/- mice.
(**A**) Parasagittal sections of representative hematoxylin-eosin staining placentas collected from wt, Tga20 and PrP-/- mice at E14.5. (d), (S), and (L) correspond to decidua, spongiotrophoblast, and labyrinth, respectively. (**B**) Correspond to Higher magnification of the labyrinth (L). Arrows and arrowheads indicate maternal (mbc) and fetal (fbc) blood cells, respectively.

Figure S9:
PrP^C expression levels affect the layer surface of different placental zones**.**
(**A** and **B**) show the proportions of the surface layer of three zones of the placenta (labyrinth; spongiotrophoblast and decidua) in normal and Cu-treated wt, Tga20 and PrP-/- mice at 14,5 and 17.5 dpc. The surfaces of the three layers were measured on parasagittal sections for each placenta. Mean values were used to calculate the mean (SEM) surface proportion of layers. (*$P < 0.05$, by ANOVA followed by Dunn's Method).

Table S1: Primers used for the real-time RT-PCR.

Movie S1: HTR organization in tube-like structures under four conditions, control; siRNA to PrP^C; Cu treatment (100 μM); siRNA to PrP^C plus Cu treatment.

2.mp4

Table S1

Genes	Forward (F)/Reverse (R)		Tm
Prion	**(F)**	**5'**-CACTGCCGAAATGTATGATGGG-**3'**	57°C
	(R)	**5'**-CAAGCCGAGTAAGCCAAAAACC-**3**'	
Mash2	**(F)**	**5'**-GGTGACTCCTGGTGGACCTA-**3'**	56°C
	(R)	**5'**-TCCGGAAGATGGAAGATGTC-**3'**	
CGm1	**(F)**	**5'**-CGATGTGAAACTGCCTCAGA-**3'**	57°C
	(R)	**5'**-CTTCCTCTGTGGAGCAGTCC-**3'**	
Proliferin	**(F)**	**5'**-TGTGTGCAATGAGGAATGGT-**3'**	54°C
	(R)	**5'**-TAGTGTGTGAGCCTGGCTTG-**3'**	
CD31	**(F)**	**5'**-GCATCGGCAAAGTGGTCAA-**3'**	58°C
	(R)	**5'**-GTTCCATTTTCGGACTGGC-**3'**	
18s	**(F)**	**5'**-TTGTTGGTTTTCGGAACTGAGGC-**3'**	59°C
	(R)	**5'**-GGCAAATGCTTTCGCTCTGGTC-**3'**	
GAPDH	**(F)**	**5'**-AACGACCCCTTCATTGAC-**3'**	57°C
	(R)	**5'**-TCCACGACATACTCAGCA-**3'**	